Oscillatory and chaotic dynamics in compartmentalized geometries

Francisco Chávez and Raymond Kapral
Chemical Physics Theory Group, Department of Chemistry, University of Toronto, Toronto, Ontario, Canada M5S 3H6
(Received 12 November 2001; published 26 April 2002)

The effects of spatial compartmentalization of a multistep reaction mechanism (Willamowski-Rössler model) whose mass action rate law shows oscillations and chaotic dynamics are explored. The mechanism is decomposed into subsets of reactions that are then assumed to take place in distinct regularly or randomly distributed spatial domains in the system. The reactive domains are coupled by diffusion. The spatiotemporal system states are investigated as a function of the system size and geometrical arrangement of the domains. A compartmentalization is chosen where the isolated domain attractors are simple steady states. It is then shown that changes in the system size or domain geometry can produce bifurcations leading to simple or period-doubled oscillatory attractors as well as chaotic states. These bifurcations are analyzed by direct simulations of the compartmentalized reaction-diffusion equations and by an analysis in terms of integral equations.

DOI: 10.1103/PhysRevE.65.056203 PACS number(s): 05.45.−a, 82.20.−w, 82.40.Bj, 02.30.Hq

I. INTRODUCTION

Spatially extended chemically reacting systems can develop a variety of spatial and temporal patterns when driven far from equilibrium [1]. On macroscopic space and time scales, the origin and nature of such patterns can be analyzed in terms of reaction-diffusion equations where reaction rates that follow from mass action kinetics are supplemented with diffusion terms. In this description one assumes that the same reaction mechanism operates in each local region of the medium. Such homogeneous media are the exception rather than the rule in nature. Most systems we encounter are inhomogeneous. The inhomogeneity can take many forms including spatial variations in system parameters, externally imposed spatial gradients, heterogeneity in the substrates on which the reactions take place, etc.

In this paper, we study some general features of a specific type of inhomogeneous chemically reacting system. We suppose that the chemical reaction mechanism comprises several elementary steps and that subsets of the elementary steps of the full mechanism take place in specific localized spatial regions. Thus, various elements of the reaction are spatially compartmentalized and these compartmentalized domains can communicate with each other by diffusion of chemical species. For such inhomogeneous media one might expect that the dynamical structure of the system will depend on geometrical factors that characterize the reactive domain configurations and the magnitudes of the diffusion coefficients of the chemical species. For example, when reactive domains are separated by distances much longer than the diffusion length, the domains will act independently. Since the reaction mechanisms differ from domain to domain, one will observe a pattern of different localized attractors. If the diffusion length is large compared to the domain distribution, the domains will act cooperatively and one will see dynamics akin to that of the full reaction mechanism.

Such compartmentalization of reaction dynamics can occur both in laboratory experiments and in nature. Laboratory examples include the Belousov-Zhabotinsky reaction carried out in microemulsions [2,3], where some reactions occur only within the micelles in the microemulsion and others occur only in the bulk of the medium. The same reaction may be carried out on specifically designed patterns in a catalytic membrane [4]. Catalytic oxidation reactions may occur on patterned platinum single-crystal surfaces [5,6]. Compartmentalization of biochemical reactions is common. Many of the reactions in the cell occur in specialized organelles or other localized regions. The effects of compartmentalization of simple models of biochemical reactions have been studied earlier. Compartmentalization can change the stability of the steady states and can influence oscillatory dynamics [7–10]. Its effects on the stationary states of a bistable system have also been investigated [11].

In this paper, we study the effects of compartmentalization on reaction kinetics whose mass action rate law gives rise to oscillatory and chaotic dynamics. Since the repertoire of possible behavior is large and investigation of the system states involves issues such as the synchronization of regular and chaotic oscillations in extended inhomogeneous media, compartmentalization can have nontrivial effects on the dynamics. In order to illustrate the phenomena we make use of the Willamowski-Rössler (WR) model [12] that exhibits a period-doubling cascade to a chaotic attractor. Section II outlines the WR mechanism, describes the particular form of the compartmentalization chosen in this study, and gives the compartmentalized reaction-diffusion equations that form the basis for the analyzes presented in the subsequent sections. A numerical study of a regular distribution of reactive domains is presented in Sec. III, while Sec. IV gives the results of an approximate analytical treatment of regular compartmentalizations, which provides insight into the observed phenomena. Section V describes the dynamical behavior of systems in which the reactive domains are randomly distributed in one- and two-dimensional media. The conclusions of the study are given in Sec. VI.

II. COMPARTMENTALIZED WILLAMOWSKI-RÖSSLER MODEL

The WR model [12] was constructed to show that a chemical mechanism that involves only bimolecular steps can yield deterministic chaotic dynamics. The mechanism

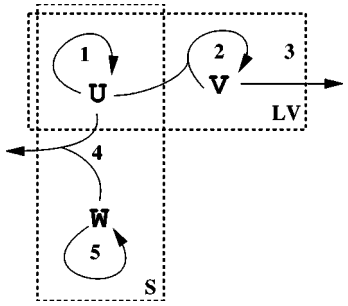

FIG. 1. Reaction network diagram of the Willamowski-Rössler oscillator. The box labeled LV comprises the Lotka-Volterra element and the box labeled *S* comprises the "switch" element.

comprises the following bimolecular steps:

$$A_1 + U \underset{k_{-1}}{\overset{k_1}{\rightleftharpoons}} 2U, \tag{1}$$

$$U + V \underset{k_{-2}}{\overset{k_2}{\rightleftharpoons}} 2V, \tag{2}$$

$$A_5 + V \underset{k_{-3}}{\overset{k_3}{\rightleftharpoons}} A_2, \tag{3}$$

$$U + W \underset{k_{-4}}{\overset{k_4}{\rightleftharpoons}} A_3, \tag{4}$$

$$A_4 + W \underset{k_{-5}}{\overset{k_5}{\rightleftharpoons}} 2W. \tag{5}$$

The species $A_1, A_2, \ldots, A_5$ are pool chemicals whose concentrations are held constant by flows of reagents into and out of the system while U, V, and W are the species whose concentrations vary with time. From the reaction network diagram for this model in Fig. 1, one sees that the WR mechanism can be viewed as a coupling between a Lotka-Volterra (LV) oscillator involving the species U and V, and "switch" (S) involving species U and W [13].

The time evolution of the concentrations is described by mass action kinetics,

$$\frac{du}{dt} = k_1 u - k_{-1} u^2 - k_2 uv + k_{-2} v^2 - k_4 uw + k_{-4}, \tag{6}$$

$$\frac{dv}{dt} = k_2 uv - k_{-2} v^2 - k_3 v + k_{-3}, \tag{7}$$

$$\frac{dw}{dt} = -k_4 uw + k_{-4} + k_5 w - k_{-5} w^2, \tag{8}$$

where the concentrations corresponding to the various species are denoted by lower case letters; e.g., $c_U = u$. The concentrations of pool species A_i may be included in the rate constants k_1, k_3, k_{-3}, k_{-4}, and k_5. We assume this has been done without change of notation.

The dynamical structure that follows from this rate law has been studied earlier and we review only some of its most important features [13]. Depending on the values of the parameters in the set $\mu = \{k_{\pm 1}, k_{\pm 2}, k_{\pm 3}, k_{\pm 4}, k_{\pm 5}\}$, this system of equations can exhibit fixed points as well as periodic and chaotic attractors in the three-dimensional concentration phase space. In the calculations presented below, we select $\mu = \{k_1 = 31.2, k_2 = 1.45, k_3 = 10.8, k_4 = 1.02, k_5 = 16.5, k_{-1} = 0.2, k_{-2}, k_{-3} = 0.12, k_{-4} = 0.01, k_{-5} = 0.5\}$ and take k_{-2} as the bifurcation parameter.

For $k_{-2} > k_{-2}^H = 0.1715$ the WR reaction has a stable fixed point. At k_{-2}^H the system undergoes a Hopf bifurcation and a period-1 limit cycle appears. A period-doubling cascade to chaos is found as k_{-2} is decreased further. For future reference, the bifurcations to period-2 and period-4 orbits occur at $k_{-2} \approx 0.1$ and $k_{-2} \approx 0.085$, respectively, while a fully developed chaotic attractor is found at $k_{-2} = 0.072$.

Given the network structure of the WR oscillator it is interesting to study a compartmentalized medium in which there are two types of reactive domain: LV domains where reactions (1), (2), and (3) take place, and S domains where reactions (1), (4), and (5) occur. The system can then be described by a reaction-diffusion equation

$$\frac{\partial \mathbf{c}(\mathbf{r},t)}{\partial t} = \mathbf{D}\nabla^2 \mathbf{c}(\mathbf{r},t) + \mathbf{R}(\mathbf{c}(\mathbf{r},t)), \tag{9}$$

subject to appropriate boundary and initial conditions. Here $\mathbf{c}(\mathbf{r},t) = \{c_k(\mathbf{r},t)\} = \{u(\mathbf{r},t), v(\mathbf{r},t), w(\mathbf{r},t)\}$ is the vector of local concentrations at time t, $\mathbf{D}$ is the diffusion coefficient matrix assumed to be constant and diagonal, and $\mathbf{R}(\mathbf{c}(\mathbf{r},t)) = \{\mathcal{R}_k(\mathbf{c}(\mathbf{r},t))\}$ is the vector of reaction rates whose elements can be written as

$$\mathcal{R}_k(\mathbf{c}(\mathbf{r},t)) = \sum_{i=1}^{N} R_k^{\{\alpha_i\}}(\mathbf{c}(\mathbf{r},t))\Theta_i(\mathbf{r}), \tag{10}$$

where $\Theta_i(\mathbf{r})$ is a characteristic function that is unity within domain i and zero otherwise and N is the total number of reactive domains. In this equation $R_k^{\{\alpha_i\}}$ is the reaction rate for species k corresponding to the subset of reactions $\{\alpha_i\}$ that occur in domain i. For the specific compartmentalization considered here, the reaction terms are

$$R_u^{LV} = k_1 u(\mathbf{r},t) - k_{-1} u(\mathbf{r},t)^2 - k_2 u(\mathbf{r},t) v(\mathbf{r},t) + k_{-2} v(\mathbf{r},t)^2,$$

$$R_v^{LV} = k_2 u(r,t) v(\mathbf{r},t) - k_{-2} v(\mathbf{r},t)^2 - k_3 v(\mathbf{r},t) + k_{-3},$$

$$R_w^{LV} = 0, \tag{11}$$

and

$$R_u^{S} = k_1 u(\mathbf{r},t) - k_{-1} u(\mathbf{r},t)^2 - k_4 u(\mathbf{r},t) w(\mathbf{r},t) + k_{-4},$$

$$R_v^{S} = 0,$$

$$R_w^{S} = -k_4 u(\mathbf{r},t) w(\mathbf{r},t) + k_{-4} + k_5 w(\mathbf{r},t) - k_{-5} w(\mathbf{r},t)^2. \tag{12}$$

In the limit of infinite diffusion the behavior is independent of the geometrical details of the medium and is equivalent to the well-mixed case. In the limit of low diffusion the reactive domains act independently and the nature of the attractors within the domains is determined by the subset of reactive steps that take place in the domains. In particular, LV domains have a single stable focus while *S* domains exhibit three different solutions: a stable node where u is almost extinct, another stable node where w almost vanishes, and an unstable node that separates the first two stable nodes. The individual reactive domains have a bifurcation structure that differs from that of the full reaction mechanism and we investigate how diffusion and geometry determine the dynamics of the compartmentalized system.

III. REGULAR DISTRIBUTION OF DOMAINS

Consider a one-dimensional medium with length L containing a simple regular distribution of alternating LV and *S* domains. The domains have length $l=L/2$ and center-to-center interdomain distance $d=L/2$. The diffusion coefficients of all species were taken to be equal, $D_u=D_v=D_w=D$. The reaction-diffusion equation was solved using an Euler scheme with periodic boundary conditions. Boundary conditions play an important role in determining the nature of the patterns seen in compartmentalized systems. Throughout the paper, with one exception discussed in Sec. IV A, we use periodic boundary conditions to model infinitely extended regular arrays of reactive domains or random distributions in large systems.

It is convenient to use scaled time and length units, $t\rightarrow t/\tau$ and $x\rightarrow x/\sqrt{D\tau}$. In terms of these scaled units, with $\tau=1$, the reaction-diffusion equation has the form in Eq. (9) with $\mathbf{D}=\mathbf{I}$, the unit matrix. The diffusion length of the system $\ell_D=\sqrt{Dt_c}$ expressed in these dimensionless units is $\ell_D\rightarrow\sqrt{t_c/\tau}$, where t_c is some characteristic time scale of the problem. A suitable choice of t_c is the period of one oscillation of the system which, for the system parameters considered below, lies in the range $1.5\geqslant t_c/\tau\geqslant 5$ and thus $1.2\geqslant\ell_D\geqslant 2.2$. Given this scaling we may investigate the behavior of the compartmentalized WR system for different values of scaled system length L. The results reported in the text and figures are presented in terms of these dimensionless space and time units; chemical concentrations are also dimensionless and determined by the values of the rate constants given in the preceding section.

Figure 2 shows the (u,v,w) phase-space trajectories of the globally averaged concentration fields projected onto the uv plane for $k_{-2}=0.11$ and different values of L. The well-mixed WR system has a period-1 limit cycle for this value of k_{-2}. While a period-1 limit cycle is observed for very small system sizes, for large L the system instead evolves to a stable fixed point determined by the stationary states of the independent LV and *S* domains. A limit cycle develops at $L=0.777$ and, as L decreases, the size of the limit cycle in phase space grows until it resembles that of the well-mixed WR system. The period of the limit cycle remains nearly constant at $T=1.74$ for $0.777<L<0.090$, the system size range that was investigated. While the phenomenon is similar in appearance to the behavior of globally averaged concentration fields in oscillatory media where dephasing occurs for large system sizes, here the nature of the local dynamics itself changes as a result of compartmentalization.

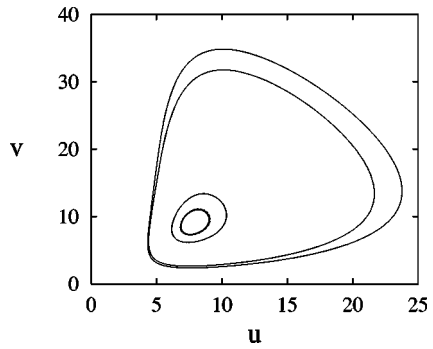

FIG. 2. Limit cycles in the compartmentalized WR system projected onto the uv plane. Concentric limit cycle loops of increasing size correspond to decreasing L ($L=0.756$, 0.730, and 0.4). The outermost cycle corresponds to that for the well-mixed WR model.

For $k_{-2}=0.095$, where a period-2 cycle exists in the well-mixed WR system, when L is much larger than the diffusion length ℓ_D, the system again evolves to a stable fixed point determined by the local stationary states of the independent LV and *S* domains. As L decreases, first a period-1 limit cycle develops. This limit cycle grows until a period-doubling bifurcation occurs and the globally averaged concentration field executes a period-2 cycle.

Figure 3 shows the globally averaged attractors for $k_{-2}=0.072$, where the well-mixed WR system has a chaotic attractor. As in the previous examples, the system size L plays the role of a bifurcation parameter and as it decreases one observes a period-doubling sequence and a chaotic attractor. In this regime the dynamics of the system is very sensitive to the system length L. For $L=0.283$ the attractor is a period-2 limit cycle, while for $L=0.2309$ it exhibits two-banded chaos.

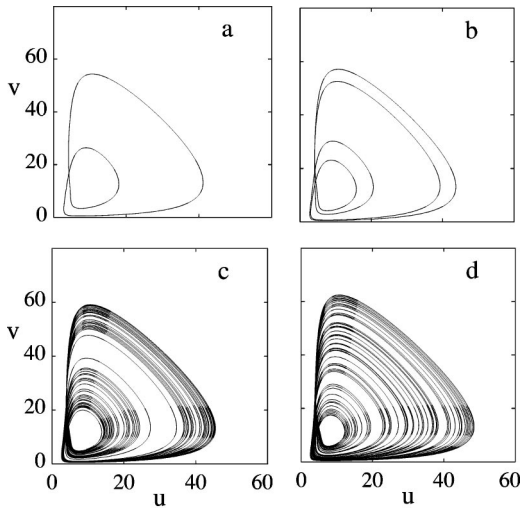

FIG. 3. Development of a chaotic attractor in the compartmentalized WR system for $k_{-2}=0.072$. Figures (a)–(d) correspond, respectively, to $L=0.283$, 0.258, 0.2309, and 0.179.

IV. INTEGRAL REPRESENTATION

A. Time-dependent case

In order to gain further insight into the nature of the dynamics in compartmentalized reacting media, it is useful to adopt an alternative approach that is based on an integral representation of the formal solution of the reaction-diffusion equation [11]. The formal solution of Eq. (9) for the concentration of species k is [14]

$$c_k(\mathbf{r},t)=\int G(\mathbf{r},t;\mathbf{r}_0,0)\,\phi_k(\mathbf{r}_0)d^s\mathbf{r}_0 + \int_0^t\int G(\mathbf{r},t;\mathbf{r}_0,t_0)\mathcal{R}_k(\mathbf{c}(\mathbf{r}_0,t_0))d^s\mathbf{r}_0dt_0 + D_k\int_0^t\oint [G(\mathbf{r},t;\mathbf{r}_0,t_0)\boldsymbol{\nabla}_{\mathbf{r}_0}c_k(\mathbf{r}_0,t_0) - c_k(\mathbf{r}_0,t_0)\boldsymbol{\nabla}_{\mathbf{r}_0}G(\mathbf{r},t;\mathbf{r}_0,t_0)]\cdot\hat{\mathbf{n}}dS_0dt_0. \quad (13)$$

The time-dependent Green function is $G(\mathbf{r},t;\mathbf{r}_0,t_0)$, $\phi_k(\mathbf{r})$ is the initial condition, $\hat{\mathbf{n}}$ is the unit vector normal to the boundary surface of the system, and dS_0 is a differential element of the surface area of the system.

Rather than considering the entire space and time-dependent concentration field, we focus on the concentration field of species k averaged over reactive domain j,

$$c_{k,j}(t)=\frac{1}{V_j}\int_{\Omega_j}c_k(\mathbf{r},t)\Theta_j(\mathbf{r})d^s\mathbf{r}, \quad (14)$$

where V_j is the volume of domain j and $\Theta_j(\mathbf{r})$ is a characteristic function that is unity within domain Ω_j and zero otherwise. Using the approximations introduced earlier [11], namely, a multipole expansion of the characteristic functions for domains different from j and an assumption of uniformity within domain j, the evolution of the domain volume average of the concentrations is given by

$$c_{k,j}(t)=I^{\phi}_{k,j}+D_kI^B_{k,j}+\sum_{i=1}^{N}\int_0^t\omega_{k,ji}(t,t_0)R_k^{\{\alpha_i\}}(\mathbf{c}_i(t_0))dt_0, \quad (15)$$

where

$$I^{\phi}_{k,j}=\frac{1}{V_j}\int\int G(\mathbf{r},t;\mathbf{r}_0,0)\,\phi_k(\mathbf{r}_0)\Theta_j(\mathbf{r})d^s\mathbf{r}_0d^s\mathbf{r}, \quad (16)$$

accounts for the effect of the initial concentration field ϕ_k, and

$$I^B_{k,j}=\frac{1}{V_j}\int_0^t\int\oint [G(\mathbf{r},t;\mathbf{r}_0,t_0)\boldsymbol{\nabla}_{\mathbf{r}_0}c_k(\mathbf{r}_0,t_0) - c_k(\mathbf{r}_0,t_0)\boldsymbol{\nabla}_{\mathbf{r}_0}G(\mathbf{r},t;\mathbf{r}_0,t_0)]\cdot\hat{\mathbf{n}}\Theta_j(\mathbf{r})dS_0d^s\mathbf{r}dt_0, \quad (17)$$

accounts for the effects arising from the system's boundaries. The prefactors $\omega_{k,ji}$ are given by

$$\omega_{k,ji}(t,t_0)=\frac{1}{V_j}\int\int_{\Omega_j}G(\mathbf{r},t;\mathbf{r}_0,t_0)d^s\mathbf{r}_0d^s\mathbf{r}\,\delta_{ji} + \int_{\Omega_j}G(\mathbf{r},t;\mathbf{r}_i,t_0)d^s\mathbf{r}(1-\delta_{ji}). \quad (18)$$

In order to proceed further the Green function must be specified. For finite one-dimensional systems, with homogeneous or zero-flux boundary conditions, the Green function may be written as an infinite series. Although calculations may be carried out for such boundary conditions, use of this complex form of the Green function obscures the analysis of the results. For this reason, we examine a simpler situation, an infinite system with zero concentrations at $x=\pm\infty$, where the Green function is given by

$$G(x,x_0;t,t_0)=\frac{\exp\left[-\dfrac{(x-x_0)^2}{4(t-t_0)}\right]}{2\sqrt{\pi(t-t_0)}}. \quad (19)$$

In writing Eq. (19) we have used the scaled variables introduced in Sec. III, where $D_k=1$ for all species k. As a result the $\omega_{k,ij}$ factors do not depend on k and we drop this symbol and refer to these quantities as ω_{ij}. Substituting this expression in Eq. (18) and performing the integrations for a medium with domains of length l separated distances d_{ij}, the prefactors are

$$\omega_{ii}(t,t_0)=\frac{2}{l}\sqrt{\frac{t-t_0}{\pi}}\{\exp[-l^2/4(t-t_0)]-1\} + \mathrm{erf}(l/2\sqrt{t-t_0}),$$

$$\omega_{ij}(t,t_0)=\frac{1}{2}\left[\mathrm{erf}\left(\frac{2d_{ij}+l}{4\sqrt{t-t_0}}\right)-\mathrm{erf}\left(\frac{2d_{ij}-l}{4\sqrt{t-t_0}}\right)\right], \quad (20)$$

where erf() is the error function.

We may now apply this general formalism to the compartmentalized WR system and, for simplicity, we set $\phi_k=0$ so that only the third term in Eq. (15) remains. We suppose that the infinite medium contains two domains, one of type LV (domain 1), and the other of type S (domain 2). Under these conditions, remembering that $R^2_v=R^1_w=0$, Eq. (15) simplifies to the set of integral equations

$$u_j(t)=\int_0^t\omega_{j1}(t-t_0)R^1_u(\mathbf{c}_1(t_0))dt_0 + \int_0^t\omega_{j2}(t-t_0)R^2_u(\mathbf{c}_2(t_0))dt_0,$$

$$v_j(t)=\int_0^t\omega_{j1}(t-t_0)R^1_v(\mathbf{c}_1(t_0))dt_0,$$

$$w_j(t)=\int_0^t\omega_{j2}(t-t_0)R^2_w(\mathbf{c}_2(t_0))dt_0, \quad (21)$$

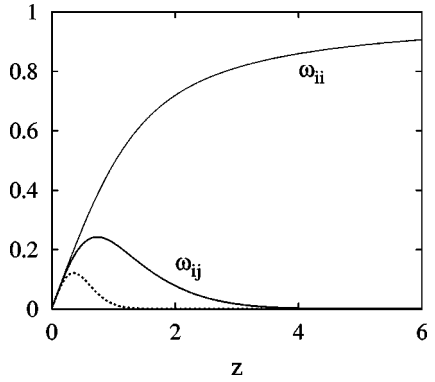

FIG. 4. Prefactors ω_{ii} and ω_{ij} as a function of z. For the off-diagonal term, the dotted line corresponds to $a=2$ and the continuous line corresponds to $a=1$.

for $j=1,2$.

Several features of these equations are worth noting. All spatial aspects of the medium are taken into account in the prefactors ω. The values of the concentrations at time t are obtained by integration of the reactive terms over all earlier times t_0, weighted by the factors ω_{ji}. Thus, the factor $\omega_{ji}(t,t_0)$ can be interpreted as the influence that the reactions in domain i at time t_0 exert on domain j at time t. It can be shown that $\omega_{jj}(t,t)=1$ and $\omega_{ji}(t,t)=0$. Making use of the change of variable $z=l/\sqrt{4(t-t_0)}$, the prefactors can be written as

$$\omega_{ii}(z)=\frac{1}{z\sqrt{\pi}}[e^{-z^2}-1]+\mathrm{erf}(z)$$

$$\omega_{ij}(z,a_{ij})=\frac{1}{2}\left\{\mathrm{erf}\left[z\left(a_{ij}+\frac{1}{2}\right)\right]-\mathrm{erf}\left[z\left(a_{ij}-\frac{1}{2}\right)\right]\right\}, \tag{22}$$

where the parameter a_{ij} is the distance between domains in units of the domain length ℓ, $d_{ij}=a_{ij}l$. Since we have only two domains, $d_{ij}\equiv al$. For nonoverlapping domains $1\leqslant a\leqslant\infty$.

The variation of the ω_{ij} with z is shown in Fig. 4. The diagonal terms ω_{ii} increase monotonically with z while each off-diagonal term ω_{ij} has a maximum. In the limit $z\to\infty$, $\omega_{ii}\to 1$, whereas the off-diagonal terms $\omega_{ij}\to 0$. In this limit we recover from Eqs. (21), the simple solutions corresponding to independent domains. However, for $z\to 0$, these equations reduce identically to $\mathbf{c}=0$, which is the concentration imposed at the boundary. The values of z corresponding to the maxima in ω_{ij} are given by

$$z_m=\sqrt{\frac{1}{2a}\ln\frac{2a+1}{2a-1}}, \tag{23}$$

and substituting this result into the definition of z, we obtain an expression for the time gap at the maxima,

$$(t-t_0)_m=\frac{al^2}{2\ln[(2a+1)/(2a-1)]}. \tag{24}$$

This time gap increases monotonically, faster than linearly, with the separation between the domains a.

We have solved Eq. (21) for values of a ranging from that for widely separated reactive domains to adjacent reactive domains. In all cases the attractor was an inhomogeneous stationary state. Figure 4 provides insight into the reason that oscillations are not observed. The self contributions from reactive domains are always much larger than the contributions from the neighboring domain when $t_0\to t$, except for very small l, but then all prefactors tend to zero and the boundaries dominate. Thus, the strong boundary effects preclude the appearance of oscillations when the reactive domains are strongly coupled.

Oscillations were found for a system with a single domain supporting the full reaction mechanism. The methodology developed above may be applied to study the effect of the domain size l on the dynamics of this isolated domain. For a large enough domain, for instance $l=63.2$, the domain-averaged concentrations execute a chaotic trajectory in phase space. For a sufficiently small l; for instance, for $l=1.414$, the system loses its oscillatory behavior and evolves to a fixed point. For intermediate lengths, we have observed limit cycles of different periodicity; e.g., a period-2 cycle is observed for $l=20$ and a period-1 cycle for $l=6.324$. This behavior is the opposite of that found for a compartmentalized medium, where the more complex behavior is seen for smaller system sizes.

B. Time-independent case

If the attractor is a stationary state, one can use the time-independent form of Eq. (15) to study the solution structure. For a finite medium of length L with two reactive domains and fixed concentrations at the boundaries, we obtain the set of equations,

$$u_j=\omega^s_{j1}R^1_u+\omega^s_{j2}R^2_u+u_0,$$

$$v_j=\omega^s_{j1}R^1_v+\omega^s_{j2}R^2_v+v_0,$$

$$w_j=\omega^s_{j1}R^1_w+\omega^s_{j2}R^2_w+w_0, \tag{25}$$

for sites $j=1,2$, where u_0, v_0, and w_0 are the concentrations at the boundaries. The superscript on the ω^s_{ij} prefactors is used to indicate that these quantities are calculated using the appropriate time-independent Green function $G(x,x_0)$,

$$G(x,x_0)=\begin{cases}\left(1-\dfrac{x_0}{L}\right)x & \text{if } x\leqslant x_0\\ \left(1-\dfrac{x}{L}\right)x_0 & \text{if } x\geqslant x_0.\end{cases} \tag{26}$$

Equations (25) are further simplified using the fact that $R^1_w=R^2_v=0$. Furthermore, setting $u_0=(u_1+u_2)/2$, $v_0=(v_1+v_2)/2$, and $w_0=(w_1+w_2)/2$, we establish periodic boundary conditions for a regular distribution of domains. Manipulating Eqs. (25) we find that the stationary solutions of the reaction-diffusion problem are given by the solutions of the set of algebraic equations,

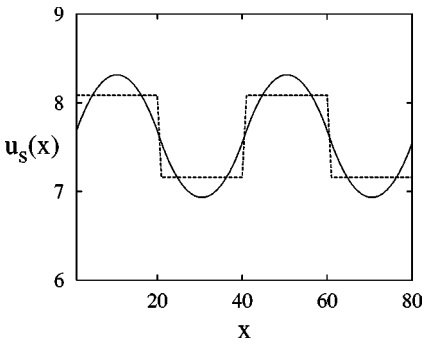

FIG. 5. Stationary spatial profile of the concentration of the u field for $k_{-2}=0.11$ and $l=0.4472$. The continuous line is the result from the direct numerical solution of the reaction-diffusion equation. The dashed line is the approximate solution for the domain-averaged concentrations using the integral representation.

$$R_v^1=0,$$

$$R_w^2=0,$$

$$R_u^1+R_u^2=0,$$

$$\gamma(R_u^1-R_u^2)=u_1-u_2, \tag{27}$$

where $\gamma=\omega_{11}^s-\omega_{12}^s=x_1 l d/L-l^2/6$ and, as usual, d is the distance between the reactive domains and l is their length. The w_{ji} prefactors for these conditions are

$$w_{ji}=\begin{cases}\left(1-\dfrac{x_j}{L}\right)x_j l-\dfrac{l^2}{6} & \text{if } x_i=x_j \\ \left(1-\dfrac{x_i}{L}\right)x_j l & \text{if } x_j<x_i,\end{cases} \tag{28}$$

where x_i denotes the position of the center of reactive domain i.

The first three equations in Eqs. (27) simply reflect the fact that the stationary state is reached when the net production/consumption of all species is zero. In addition, it can be shown that $v_1=v_2$ and $w_1=w_2$; thus, the solution of the system of equations (27) gives the six stationary state concentrations of the problem.

The validity of the approximations made in the course of developing these equations can be tested in several ways. For instance, for $\gamma=0$ we obtain $u_1=u_2$ and recover the well-mixed case. Also, notice that for $\gamma=\infty$, we obtain from Eqs. (27) that $R_u^1=R_u^2=0$, i.e., each domain attains its local stationary state independently.

For intermediate values of γ one can solve Eqs. (27) and compare with the numerical solution of the reaction-diffusion equations in nonoscillatory regimes. Good agreement is found. Figure 5 shows the results for $k_2=0.11$ and $l=0.4472$. This domain length is too large to support oscillations in the compartmentalized medium and the system rapidly evolves to the final stationary spatial profile exhibited in the figure. Only the profile for u is shown but similar agreement is found for all other concentration fields. The stationary concentrations u_s, v_s, and w_s averaged over the S and LV domains are presented in Table I

TABLE I. Comparison of the concentrations averaged over the different types of domain, obtained by solving the reaction-diffusion (RD) equations and the integral representation approximation (Integral).

	u_s	v_s	w_s
LV (RD)	7.157	8.489	18.401
LV (Integral)	7.158	8.511	18.398
S (RD)	8.083	8.508	18.374
S (Integral)	8.084	8.511	18.398

Equations (27) can be used to obtain an estimate of the value of the length of the domain corresponding to the onset of oscillations. For large values of l, these equations exhibit three solutions. Two of the solutions collide at a critical value of l, l_c, leaving only one real solution. For the system considered in this section we find $l_c=0.40$, which is to be compared with $l_c=0.38$, the numerical estimate of the critical value obtained from the simulation of the reaction-diffusion equation.

V. RANDOM DISTRIBUTION OF DOMAINS

A. One-dimensional media

We have also studied random distributions of LV and S reactive domains. The one-dimensional random medium was constructed in the following way. The total number of reactive domains was fixed at N. A number N of points was chosen at random from a uniform distribution on $[0,L]$ and each point was taken to be the center of an LV or S reactive domain of length l. The domain types, LV and S, were chosen with probabilities p and $1-p$, respectively, allowing overlapping of domains if the distance between two centers was less than l. The overlapping regions were assumed to support the full WR reaction mechanism and constitute a third type of reactive domain with label C. The value of $k_{-2}=0.072$, where the well-mixed system is in the chaotic regime, was chosen for all of the one- and two-dimensional simulations reported in this section.

Even though N is fixed, since domains may overlap, fluctuations exist in the densities of reactive domains. The densities of each type of domain are denoted by ρ_I, ρ_{LV}, ρ_S, and ρ_C, for inactive LV, S, and C domains, respectively, where $\rho_J=L_J/L$ with L_J the length occupied by domains of type J. Also, although LV and S domains with a fixed length l are randomly placed in the system, due to the fact that domains may overlap to generate type-C domains, the domains that result from this random process do not have a constant length, in contrast with the regular domain configurations considered in the previous sections.

The evolution of the WR system with such random compartmentalization was investigated. Different realizations of the random process were generated for a system of size L, taking $l=L/50$ and $p=0.5$. Two values of N were considered: $N=26$, where there is a very low average density of

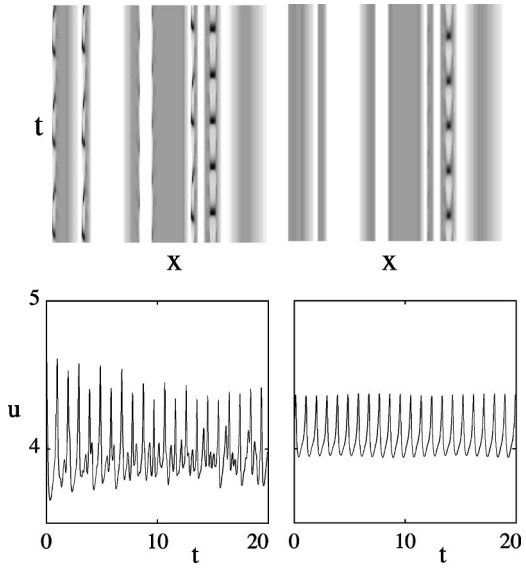

FIG. 6. Space-time plots for one realization of the random medium for $N=26$ and $L=200$ (top left) and $L=115.47$ (top right). Time increases from bottom to top; time interval of five, time units shown. The gray shades code the magnitudes of the u field. The globally averaged u fields versus time corresponding to these two systems are shown in the lower left and right panels, respectively, of this figure.

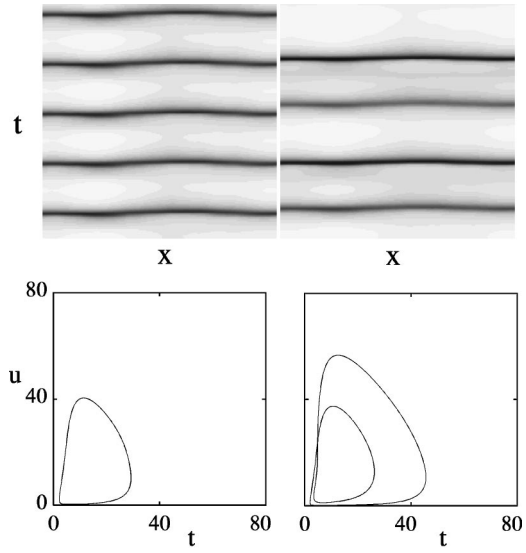

FIG. 7. Space-time plots of the random medium for $N=26$ for small L: $L=2.82$ (upper left) and $L=2.39$ (upper right). Coding is the same as that in Fig. 6. A time interval of twenty, time units is shown in both panels. Phase plane plots of the globally averaged u and v fields for the systems shown in the upper panels: $L=2.82$ (lower left), $L=2.39$ (lower right).

overlapping sites $\langle \rho_C \rangle = 0.053$, and $N=80$, where $\langle \rho_C \rangle = 0.43$. Here the angular brackets refer to an average over realizations of the random compartmentalization process.

For systems with low $\langle \rho_C \rangle = 0.053$, in the limit of large L, the dynamics on LV and S domains evolves to the stationary states that are determined by the partial WR mechanisms that operate on these domain types. However, oscillations are observed on the C domains where the full WR mechanism operates. This behavior is seen in the space-time plots shown in the top two panels of Fig. 6 for one realization of the random compartmentalization. The realization for $L=200$ shown in this figure has six oscillating domains (left panel). Since the scaled diffusion length ℓ_D is fixed, as L decreases, the oscillations are no longer confined to the C domains but extend into the neighboring LV and S domains. These oscillating centers emit waves that are quickly dissipated in the surrounding medium. The oscillations in this regime are localized and their period is short; e.g., the period averaged over five realizations of the random process is $\langle T \rangle = 0.89$ while the period for bulk oscillations is several times longer. For the same domain configuration as in the upper left panel of Fig. 6, for $L=115.47$, one sees that the oscillations in five of these domains have been extinguished (upper right panel). For smaller values of L, oscillations in all domains are extinguished and the system exhibits a stable nonuniform stationary state. Although the qualitative aspects of the behavior described above do not depend strongly on the particular realization of the random medium, the spatial profile of the stationary state does depend on the geometric details of the realization.

Further decrease of L leads to a region of global oscillations when $L \approx \ell_D$. These oscillations are different from those observed for larger values of L. The dynamics depends more sensitively on the detailed geometry of the realization: the phase-space shape of the global attractor can vary and some realizations may not even exhibit oscillations. For example, only two out of five realizations exhibited global oscillations with average period $\langle T \rangle = 4.72$, five times larger than that in the large L regime. In this regime diffusion is strong enough to yield coherent oscillations over the entire medium (see Fig. 7).

For systems with a higher average density of overlapping domains $\langle \rho_C \rangle = 0.43$, the medium contains larger clusters of C domains and clusters close to each other tend to synchronize. The left panel of Fig. 8 shows a space-time plot of the dynamics in this regime for $L=200$. The three oscillating regions near the right border of the system are synchronized, while the two oscillating regions near the left border emit waves. For intermediate values of L the nonoscillatory regime discussed above for the low concentration case is not

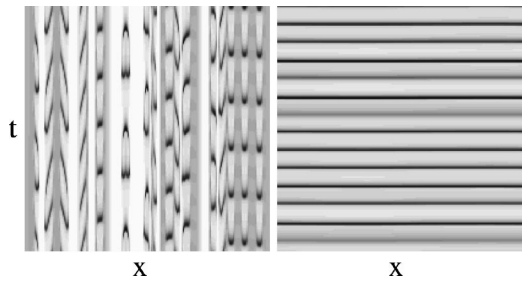

FIG. 8. Space-time plots for one realization of the random medium for $N=80$: $L=200$, time interval of five, time units shown (left) and $L=0.70$, time interval of twenty, time units shown (right) which corresponds to Fig. 9 (lower right). Coding is the same as that in Fig. 6.

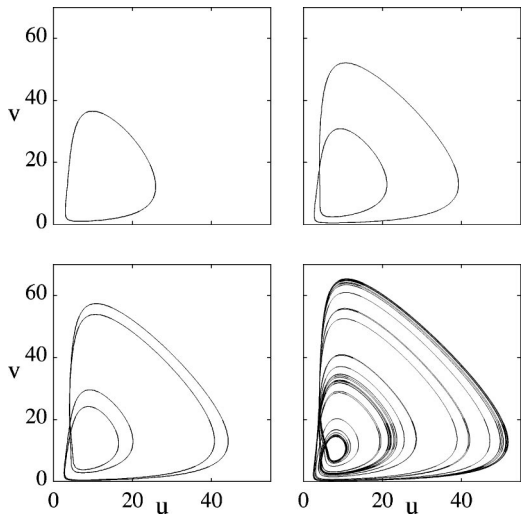

FIG. 9. Phase plane plots of the globally averaged u and v fields for $N=80$ and $L=2.0$ (upper left), 1.41 (upper right), 1.15 (lower left), and 0.70 (lower right).

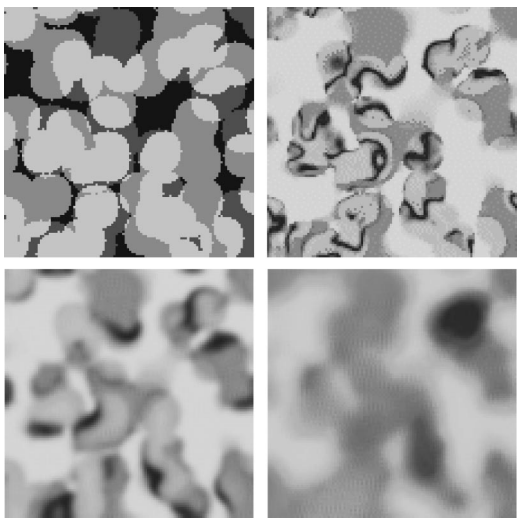

FIG. 10. Top left: One realization of the random configuration of LV, *S*, and *C* domains. The domain type is color coded by shades of gray; the darkest shades correspond to inactive areas of the medium and the lightest to *C*-type overlapping domains. The other panels are instantaneous configurations of the u field for $L=112$ (top right), 35.42 (bottom left), and $L=11.20$ (bottom right). The magnitude of u is proportional to the intensity of gray shade.

observed and globally synchronized oscillations occur in most of the realizations. The period of the global oscillations, averaged over five realizations of the random process, was found to be $\langle T\rangle=1.36$, which is considerably faster than that for low ρ_C. This behavior is expected since a larger proportion of *C* domains should lead to faster global dynamics; however, it is still true that the phase-space shapes of the observed attractors depend on the details of the domain distribution. The right panel of Fig. 8 is a space-time plot when the system is in the globally synchronized chaotic regime. Figure 9 shows the global attractors for a particular realization for different sizes of the system. The globally averaged dynamics shows a partial period-doubling cascade and a chaotic attractor corresponding to the dynamics in the right panel of Fig. 8.

B. Two-dimensional media

A two-dimensional random compartmentalized medium can be constructed by placing a total of N circular domains of radius r at random in a system of size $L\times L$ with periodic boundary conditions. Again, the discs are chosen to be of type LV with probabiliy $p=0.5$ and *S* with probability $1-p$. The overlapping regions are of type *C*, where the full WR mechanism operates.

The upper left panel in Fig. 10 shows one realization of the random medium for $N=80$ and $r=L/11.2$. The domain type is color coded by gray shades (see caption). In this realization the densities of the different domains are $\rho_I=0.1236$, $\rho_{LV}=0.1432$, $\rho_S=0.2894$, and $\rho_C=0.4438$. The total area fraction covered in this realization is $\rho_{LV}+\rho_S+\rho_C=\rho_T=0.8764$. The Johnson-Mehl-Avrami (JMA) equation, which has been used extensively in the materials science literature [15,16], expresses ρ_T in terms of the extended area fraction ρ_e as

$$\rho_T=1-e^{-\rho_e}, \tag{29}$$

where ρ_e is the area fraction covered by the circles ignoring overlapping, $\rho_e=N\pi r^2/L^2$. In our realization the JMA equation yields $\rho_e=0.8650$. The percolation threshold ρ_T^* for overlapping circles has been determined earlier by means of computer simulations [17] and Monte Carlo position space renormalization group calculations [18]. The results in the literature give a value of ρ_T^* between 0.67 and 0.688, thus our medium exhibits an area fraction covered well above the threshold. However, while the discs percolate the overlapping *C*-type regions do not. In the figure one can see that the medium contains six large clusters of *C* domains and a few additional smaller ones.

The remainder of the panels in this figure show instantaneous configurations of the concentration field u for different values of the system size: $L=112$ (top right), 35.42 (bottom left), and $L=11.20$ (bottom right). The evolution of the system for large L is characterized by a sequence of concentration fronts propagating within the overlapping clusters. The fronts are generated at the borders of the clusters and propagate until they collide and annhilate with an incoming front or reach another border. The shapes of these fronts are irregular and are dictated by the shapes of the borders where they are generated. Diffusive coupling is not strong enough to homogeneize the interiors of the clusters. The clusters of LV and *S* domains attain their steady states and are only weakly affected by the activity inside the *C* clusters. The time series of the globally averaged u field is characterized by irregular oscillations of short period and small amplitude. As L decreases larger regions of the medium synchronize. The clusters of *C* domains cease emitting pulses and begin oscillating uniformly and act as pacemakers. In Fig. 10 (bottom right), one such large pacemaker is visible near the upper-right corner. If L is decreased further diffusive cou-

pling is able to synchronize the entire medium and the system enters a regime of global oscillations, which have long period and large amplitude.

VI. CONCLUSIONS

When the reaction mechanism comprises several steps and can support oscillatory or chaotic dynamics, compartmentalization can lead to a variety of spatiotemporal states not observed either in the underlying well-mixed system or in the reaction-diffusion system without compartmentalization. The complexity of these systems arises from the interplay between the compartmentalization of specific subsets of the reaction mechanism in distinct spatial domains and the diffusive coupling among such domains. We have shown how system size or diffusion and domain geometry can act as bifurcation parameters to produce new spatiotemporal states. The results show that the spatial and temporal patterns observed in a given system are determined by geometrical factors. As a result one cannot simply deduce the nature of the dynamics from a knowledge of the mass action kinetics that follows from the reaction mechanism.

The WR mechanism and the specific compartmentalization we have studied in some detail in this paper should be regarded as an illustration, that demonstrates the types of phenomena that can be seen in compartmentalized reaction-diffusion systems in the far-from-equilibrium domain. As such, even though this system was chosen because it exhibits a variety of attractors in its well-mixed form, a restricted perspective was taken in some parts of the study. Compartmentalization often entails not only partitioning of reactive steps of the mechanism in spatial domains, but also concomitant changes of the diffusion coefficients of chemical species in the different domains. Our investigations intentionally have made the simplifying assumption that diffusion coefficients are the same for all species and are independent of spatial coordinates. This has allowed us to focus on effects arising solely from compartmentalization of the reaction mechanism. When spatial variations in diffusion coefficients are accounted for, new dynamics is likely to arise.

Compartmentalized geometries can play a role in reactions on composite catalytic surfaces, in microemulsions or other inhomogeneous media, and cellular biological systems; thus, the phenomena we have described in this paper can be sought in experiments on chemical and biochemical systems. In this work we have chosen to use a set of scaled dimensionless variables in terms of which the diffusion coefficient is $D=1$. The system size in dimensional units $\overline{L}$ is given by $\overline{L}=\sqrt{D\tau}L$ and the diffusion length by $\overline{\ell}_D=\sqrt{D\tau}\ell_D$. The values of diffusion coefficients in systems of interest can vary widely, depending on the nature of the medium (solution, gel, solid surface, cell) in which diffusion takes place, and the characteristic reaction times can also vary widely. The space scales in systems of interest typically vary from μm to cm ranges. Since many of the phenomena we have described arise from accessible length scale, diffusion or geometrical factor changes, the bifurcations discussed above should be observable in experimental studies designed to probe the spatiotemporal dynamics of such systems. It is now often possible to taylor the geometrical features of inhomogeneous media, making it possible to probe the bifurcation structure that arises from geometrical features, such as the differences between regular and random domain configurations. The work presented here should provide guides to such studies.

ACKNOWLEDGMENT

This work was supported in part by a grant from the Natural Sciences and Engineering Research Council of Canada.

[1] *Chemical Waves and Patterns*, edited by R. Kapral and K. Showalter (Kluwer, Dordrecht, The Netherlands, 1995).
[2] V.K. Vanag and I.R. Epstein, Phys. Rev. Lett. **87**, 228301 (2001); Science **294**, 835 (2001).
[3] V.K. Vanag and I. Hanazaki, J. Phys. Chem. A **101**, 2147 (1997).
[4] O. Steinbock, P. Kettunen, and K. Showalter, Science **269**, 1857 (1995).
[5] J. Wolff, A.G. Papathanasiou, I.G. Kevrekidis, H.H. Rotermund, and G. Ertl, Science **294**, 134 (2001).
[6] M. Bär, A.K. Bangia, I.G. Kevrekidis, G. Haas, H.H. Rotermund, and G. Ertl, J. Phys. Chem. **100**, 19 106 (1996).
[7] L. Glass and S.A. Kauffman, J. Theor. Biol. **39**, 103 (1973).
[8] R.M. Shymko and L. Glass, J. Chem. Phys. **60**, 835 (1974).
[9] L. Glass and R. Pérez, J. Chem. Phys. **61**, 5242 (1974).
[10] H.D. Thames, J. Theor. Biol. **41**, 331 (1973).
[11] F. Chávez and R. Kapral, Phys. Rev. E **63**, 016211 (2001).
[12] K.-D. Willamoski and O.E. Rössler, Z. Naturforsch. A **35A**, 317 (1980).
[13] B.D. Aguda and B.L. Clarke, J. Chem. Phys. **89**, 7428 (1988).
[14] R. Haberman, *Elementary Partial Differential Equations with Fourier Series and Boundary Value Problems* (Prentice Hall, New York, 1997); I. Stakgold, *Green's Functions and Boundary Value Problems* (Wiley, New York, 1998).
[15] W.A. Johnson and R. Mehl, Trans. AIME **135**, 416 (1939).
[16] M. Avrami, J. Chem. Phys. **7**, 1103 (1939); **8**, 212 (1940); **8**, 177 (1941).
[17] E.T. Gawlinsky and H.E. Stanley, J. Phys. A **14**, L291 (1981).
[18] T. Vickseck and J. Kertész, J. Phys. A **14**, L31 (1981).